Topological transition between competing orders in quantum spin chains

Shintaro Takayoshi, Shunsuke C. Furuya, and Thierry Giamarchi

Phys. Rev. B **98**, 184429 — Published 27 November 2018

DOI: 10.1103/PhysRevB.98.184429

Topological transition between competing orders in quantum spin chains

Shintaro Takayoshi,[1,2] Shunsuke C. Furuya,[3] and Thierry Giamarchi[1]

[1] *Department of Quantum Matter Physics, University of Geneva, Geneva 1211, Switzerland*
[2] *Max Planck Institute for the Physics of Complex Systems, Dresden 01187, Germany*
[3] *Condensed Matter Theory Laboratory, RIKEN, Wako, Saitama 351-0198, Japan*

(Dated: October 10, 2018)

We study quantum phase transitions between competing orders in one-dimensional spin systems. We focus on systems that can be mapped to a dual-field double sine-Gordon model as a bosonized effective field theory. This model contains two pinning potential terms of dual fields that stabilize competing orders and allows different types of quantum phase transition to happen between two ordered phases. At the transition point, elementary excitations change from the topological soliton of one of the dual fields to that of the other, thus it can be characterized as a topological transition. We compute the dynamical susceptibilities and the entanglement entropy, which gives us access to the central charge, of the system using a numerical technique of infinite time-evolving block decimation and characterize the universality class of the transition as well as the nature of the order in each phase. The possible realizations of such transitions in experimental systems both for condensed matter and cold atomic gases are also discussed.

I. INTRODUCTION

Low dimensional quantum magnets show rich phase diagrams due to the interplay between strong correlations and quantum fluctuations. This competition is at the root of the existence of phases with very different physics, separated by quantum phase transitions when parameters of the system are varied. In one dimensional (1D) quantum magnets, these transitions often have a topological nature. The simplest example of such a transition is the one between a massless phase dominated by XY correlations and the massive Ising phase existing in an anisotropic Heisenberg spin-1/2 chain. The universality class of this transition is the celebrated Berezinskii-Kosterlitz-Thouless (BKT) transition [1–3], which is characterized by a set of topological excitations. A field theoretical description is instrumental in understanding the properties of such transitions. In the above mentioned case, the corresponding field theory is the sine-Gordon model [4] and the low-energy excitations are solitons and carry a topological index. Another example of system described by the sine-Gordon theory is the Heisenberg chain with a staggered magnetic field such as Cu benzoate [5–7]. A field theoretical approach to topological phases has been used with success for more complicated phases, e.g. the Haldane phase in $S = 1$ quantum spin chains [8, 9].

In this paper, we focus on the phase transitions in quantum magnets which are caused by the competition between two dual fields having a topological nature. Such systems are mapped onto a dual-field double sine-Gordon (DDSG) model [10–13]. This model contains two different potential terms pinning the dual fields. If the strength of these potentials is varied, the stabilized order is changed and a quantum phase transition occurs. In addition to quantum magnets, the DDSG model appears in a broad context such as in XY models with symmetry breaking fields, in mixtures of electric charges and magnetic monopoles [14, 15], and in quantum ladder systems [16–18]. Experimentally the DDSG model has been realized in the material $BaCo_2V_2O_8$ [19]. This compound has a strong Ising anisotropy and when an external uniform magnetic field is applied, an effective staggered field is introduced in the direction perpendicular to both the anisotropy axis and the external magnetic field. Thus the Néel orders along the anisotropy axis and along the effective staggered field are competing in this system. The quantum phase transition between them can be triggered by increasing the strength of the external magnetic field, and it is measured directly in inelastic neutrons scattering (INS) experiments.

In the following, we examine various possible realizations of the DDSG model in quantum magnets, and study quantitatively the resulting transitions. We combine the field theory with a numerical analysis based on the infinite time-evolving block decimation (iTEBD), which utilizes a matrix product state (MPS) such as the density matrix renormalization group [20]. We compute various observables such as the staggered magnetization, the entanglement entropy and the dynamical spin-spin susceptibility. In particular, the dynamical susceptibility not only has a theoretical interest but also is directly related with the experiments such as inelastic neutron scattering (INS), electron spin resonance (ESR), and nuclear magnetic resonance (NMR).

This paper is organized as follows. In Sec. II, we quickly review the bosonization and give some examples of quantum spin systems described by the DDSG model. In Sec. III, we study the quantum phase transition between competing orders using the examples given in Sec. II. Section IV discusses how the dynamical susceptibility changes below and above the transition. Section V is devoted to discussing applications to real materials. We summarize our results and discuss future problems in Sec. VI.

II. BOSONIZATION AND DUAL-FIELD DOUBLE SINE-GORDON MODEL

In this section, we briefly review the bosonization of 1D spin chains [4]. We map the spin operators to bosonic scalar fields using the formula,

$$\begin{aligned} S^z_j &= -\frac{a}{\pi}\frac{d\phi(x)}{dx} + a_1(-1)^j\cos(2\phi(x)) + \cdots, \\ S^+_j &= e^{-i\theta(x)}[b_0(-1)^j + b_1\cos(2\phi(x)) + \cdots], \end{aligned} \tag{1}$$

where $x = ja$ is a spatial coordinate (a is the lattice constant) and a_0, b_0 and b_1 are nonuniversal constants which can be estimated numerically [21–24] $\phi(x)$ and $\theta(x)$ are dual bosonic fields satisfying the commutation relation $[\phi(x), \theta(x')] = -i\pi\vartheta_{\rm step}(x-x')$ ($\vartheta_{\rm step}(x-x')$ is the step function). The fields $2\phi(x)$ and $\theta(x)$ can be intuitively interpreted as polar and azimuthal angles of the staggered magnetization.

The Hamiltonian of Heisenberg chains with an Ising anisotropy (XXZ models)

$$\mathcal{H}_{\rm XXZ} = J\sum_j (S^x_j S^x_{j+1} + S^y_j S^y_{j+1} + \Delta S^z_j S^z_{j+1}) \tag{2}$$

is bosonized as

$$\begin{aligned} \mathcal{H}^{\rm eff}_{\rm XXZ} = \frac{v}{2\pi}\int dx \Big[\frac{1}{K}\Big(\frac{d\phi(x)}{dx}\Big)^2 + K\Big(\frac{d\theta(x)}{dx}\Big)^2\Big] \\ - \lambda\int dx\cos(4\phi(x)) + \cdots, \end{aligned}$$

where λ is some constant, v is spinon velocity, and K is the Luttinger parameter. The $\cos(4\phi(x))$ term has the scaling dimension $4K$, and it is relevant in the Ising anisotropic ($\Delta > 1$, $K < 1/2$) region. It works as a potential to pin the field $\phi(x)$. When $\phi(x)$ is fixed at $n\pi/2$ (n: integer), the system has Néel order along the z axis and the excitations are gapped. If we add a pinning potential for $\theta(x)$, it competes with the $\phi(x)$ pinning potential, since $\phi(x)$ and $\theta(x)$ are conjugate they cannot be simultaneously fixed. The resulting model is the DDSG model,

$$\begin{aligned} \mathcal{H}_{\rm DDSG} = \frac{v}{2\pi}\int dx \Big[\frac{1}{K}\Big(\frac{d\phi(x)}{dx}\Big)^2 + K\Big(\frac{d\theta(x)}{dx}\Big)^2\Big] \\ - g_1\int dx\cos(m\phi(x)) - g_2\int dx\cos(n\theta(x)). \end{aligned} \tag{3}$$

where m and n are integers and g_1, g_2 are nonuniversal constants.

In the following, we study several microscopic situations for which the bosonized field theory is a DDSG model.

A. XXZ model with a staggered magnetic field along the x direction

Let us add a staggered magnetic field along the x axis $-h_x\sum_j(-1)^j S^x_j$ to the XXZ model (2). This staggered field is bosonized as

$$-h_x\sum_j(-1)^j S^x_j = -h_x b_0\int dx\cos\theta(x) + \cdots.$$

The $\cos\theta(x)$ term has a scaling dimension $1/(4K)$ and is relevant for $K > 1/8$. Therefore, the total bosonized Hamiltonian is the DDSG model (3) with $m = 4$, $n = 1$. For $\Delta > 1$ and $h_x = 0$, the ground state has Néel order (staggered magnetization) along the z axis and the ϕ field is pinned. Since $\cos\theta(x)$ dominates over $\cos(4\phi(x))$ with increasing h_x and the θ field is pinned, there is a quantum phase transition. The staggered field h_x immediately creates a finite staggered magnetization along the x axis, but the staggered magnetization along the z axis becomes 0 in the high h_x phase and thus works as an order parameter. Note that we could also use $\langle\cos(\nu\theta(x))\rangle$ as an order parameter, where ν is any noninteger number (for example $\nu = 1/2$) since it becomes zero in the ϕ pinned phase and nonzero only in the high field phase. Such order parameter is however nonlocal in terms of the spin operators [25] and thus its measurement can only be done in particular systems, as is discussed in Sec. V. Using the spin current operator [4]

$$\mathcal{J}^{\rm s}_j \equiv \frac{i}{2}(S^+_j S^-_{j+1} - S^-_j S^+_{j+1}) = -vK\frac{a}{\pi}\frac{d\theta(x)}{dx} + \cdots,$$

$\cos(\nu\theta(x))$ is represented as

$$\cos\Big(\frac{\nu\pi}{vK}\sum_{l=-\infty}^{j}\mathcal{J}^{\rm s}_l\Big) = \cos\Big(\nu\int_{-\infty}^{x}dx'\frac{d\theta(x')}{dx'}\Big) + \cdots.$$

Thus nonlocal measurements are needed for the experimental observation of $\langle\cos(\nu\theta(x))\rangle$. For quantities related to particle density (or S^z), such nonlocal quantity could be measured in cold atomic systems (see Sec. V B).

Another order parameter which is local and can thus be directly measured in condensed matter experiments is the staggered magnetization $\cos(2\phi(x))$. The lowest energy excitation is a soliton of the $\phi(x)$ ($\theta(x)$) field in the low (high) h_x phase. The phase properties are summarized in Table I.

TABLE I. Summary of the phase properties of the XXZ model with a staggered magnetic field in the x direction.

	low h_x phase	high h_x phase
pinned field	$\phi(x)$	$\theta(x)$
$\langle\cos(2\phi(x))\rangle \propto \langle\sum_j(-1)^j S^z_j\rangle$	$\neq 0$	0
$\langle\cos\theta(x)\rangle \propto \langle\sum_j(-1)^j S^x_j\rangle$	$\neq 0$	$\neq 0$
$\langle\cos(\nu\theta(x))\rangle$ (ν: noninteger)	0	$\neq 0$
soliton	$\phi(x) = 0 \to \pi/2$	$\theta(x) = 0 \to 2\pi$

B. XXZ model with XY anisotropy

Let us now consider another type of perturbation to the XXZ chain, which is the XY anisotropy. When such

a term is bosonized, it has the form of

$$D_{xy}\sum_j (S^x_j S^x_{j+1} - S^y_j S^y_{j+1}) = -D_{xy} c_1 \int dx \cos(2\theta(x)) + \cdots ,$$

where c_1 is a nonuniversal constant. The $\cos(2\theta(x))$ term has the scaling dimension $1/K$ and it is relevant for $K > 1/2$. The total bosonized Hamiltonian is the DDSG model (3) with $m = 4$, $n = 2$, instead of $m = 4$ and $n = 1$ of the previous section. In this case, the two cosine potential terms are simultaneously marginal at $K = 1/2$, and a controlled perturbative renormalization can be constructed [10] around the marginal point. The properties of such a transition will thus be quite different and are summarized in Table II.

TABLE II. Summary of the phase properties in the XXZ model with XY anisotropy.

	low D_{xy} phase	high D_{xy} phase
pinned field	$\phi(x)$	$\theta(x)$
$\langle\cos(2\phi(x))\rangle \propto \langle\sum_j (-1)^j S^z_j\rangle$	$\neq 0$	0
$\langle\cos\theta(x)\rangle \propto \langle\sum_j (-1)^j S^x_j\rangle$	0	$\neq 0$
soliton	$\phi(x) = 0 \to \pi/2$	$\theta(x) = 0 \to \pi$

C. Other perturbations

Although we focus mostly on the two above mentioned models below, it is also possible to consider other perturbations such as a staggered field along z axis $-h_z \sum_j (-1)^j S^z_j$ and a dimerization $\delta \sum_j (-1)^j \boldsymbol{S}_j \cdot \boldsymbol{S}_{j+1}$. These perturbations are bosonized as

$$-h_z \sum_j (-1)^j S^z_j = -h_z a_1 \int dx \cos(2\phi(x)) + \cdots ,$$

$$\delta \sum_j (-1)^j \boldsymbol{S}_j \cdot \boldsymbol{S}_{j+1} = \delta d_1 \int dx \sin(2\phi(x)) + \cdots .$$

These terms give another type of DDSG model, but some of them can be related through a transformation since the fields ϕ and θ can be rescaled by the transformation

$$\begin{aligned} \phi &\to b\phi \\ \theta &\to \frac{1}{b}\theta \end{aligned} \tag{4}$$

that preserves the commutation relation. For example, the Heisenberg model with a staggered z field and XY anisotropy is equivalent to the DDSG model (3) with $m = 2$, $n = 2$. This can be mapped to the $m = 4$, $n = 1$ case through the transformation $\phi \to 2\tilde{\phi}$, $\theta \to \tilde{\theta}/2$, $K/4 \to \tilde{K}$. However the operators that correspond to local observable are different since the formula (1) is unchanged.

III. QUANTUM PHASE TRANSITION BETWEEN COMPETING ORDERS

In this section, we study the properties of the quantum phase transition between competing orders for the models mentioned in Sec. II.

First, we consider the XXZ model with staggered x field,

$$\mathcal{H} = \mathcal{H}_{\rm XXZ} - h_x \sum_j (-1)^j S^x_j . \tag{5}$$

In Fig. 1(a), we show the staggered magnetization per site $m^{x(z)}_{\rm N}$ along $x(z)$ axis calculated by iTEBD. The phase transition is characterized by the disappearance of $m^z_{\rm N}$, and the critical field is $h_{x,{\rm c}}/J \simeq 0.071$. Let us determine the universality class of this transition. In Fig. 2(a), we show the log-log plot of the order parameter $m^z_{\rm N}$ as a function of $h_{x,{\rm c}} - h_x$. The fitting function is given as $m^z_{\rm N} = 1.055((h_{x,{\rm c}} - h_x)/J)^{0.129}$, and the critical exponent is $\beta = 0.129 \simeq 1/8$. We also calculate the entanglement entropy for a finite interval. When the system is bipartitioned into the subsystems A and B, where A is an interval consisting of l spins and B is the remainder, the reduced density matrix of the subsystem A is defined as $\rho_A = {\rm Tr}_B |\Psi\rangle\langle\Psi|$ ($|\Psi\rangle$ is the ground state). Then the entanglement entropy is represented as $S_{\rm EE} = {\rm Tr}\rho_A \ln \rho_A$. In systems described by a conformal field theory, the entanglement scales as [26]

$$S_{\rm EE} = \frac{c}{3} \ln l + {\rm const}, \tag{6}$$

where c is the central charge. The entanglement entropy $S_{\rm EE}$ as a function of the subsystem size l that is calculated at the transition point $h_{x,{\rm c}}$ is shown in Fig. 2(b). When the data are fitted by (6), the function is $S_{\rm EE} = 0.157 \ln l + 0.892$ and the central charge is estimated as $c = 0.471 \simeq 1/2$. These results $\beta \simeq 1/8$ and $c \simeq 1/2$ indicate that the transition belongs to the Ising universality class. In terms of a field theory, the DDSG model is equivalent to two Majorana fermions [11, 27]. At the transition point, one of the Majorana fermions

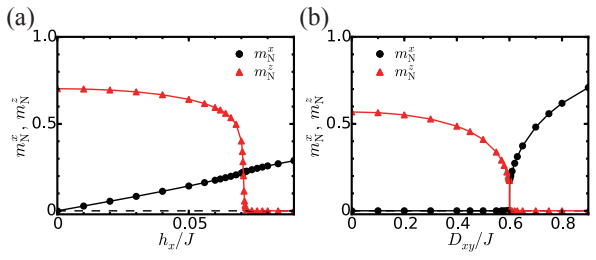

FIG. 1. Staggered magnetization curves for $m^x_{\rm N}$ and $m^z_{\rm N}$ in the XXZ model with (a) staggered x field ($\Delta = 1.9$) and (b) XY anisotropy ($\Delta = 1.6$). The saturation value of $m^{x(z)}_{\rm N}$ is normalized to 1.

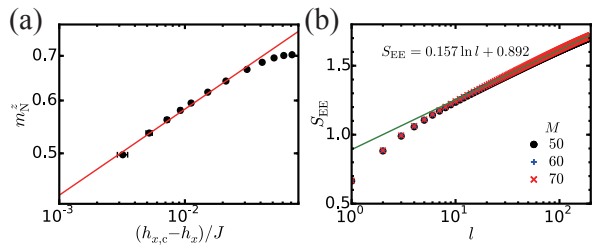

FIG. 2. (a) Log-log plot of $m_{\rm N}^z$ as a function of $h_{x,c} - h_x$. (b) Semi-log plot of entanglement entropy for a finite interval $S_{\rm EE}$ as a function of the size of the interval l at $h_x = h_{x,c}$. M is the bond dimension of MPS (see Appendix A).

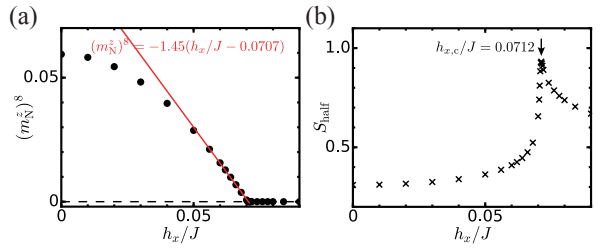

FIG. 3. Plot of (a) $(m_{\rm N}^z)^8$ (b) half-infinite entanglement entropy $S_{\rm half}$ as a function of h_x.

is gapped out while the other remains gapless, thus the transition is of the Ising type.

In Fig. 2(a), we see that the data points are deviated from the fitting line in the region of and $(h_{x,c} - h_x)/J \gtrsim 0.03$. Let us comment on this point. Figure 3(a) shows the plot of $(m_{\rm N}^z)^8$ as a function of h_x. The solid line represents a linear fitting, and data points are away from the line in $h_x/J \leq 0.04$. This indicates that the deviation in the region of $(h_{x,c} - h_x)/J \gtrsim 0.03$ in Fig. 2(a) is due to getting away from the critical region. From the equation of the fitting line $(m_{\rm N}^z)^8 = -1.45(h_x/J - 0.0707)$, the critical field is obtained as $h_{x,c}/J = 0.0707$. We can also determine $h_{x,c}$ from the divergence of half-infinite entanglement entropy $S_{\rm half}$, which is calculated by the bipartition of the system into two half-infinite chains. In Fig. 3(b), we plot the half-infinite entanglement entropy $S_{\rm half}$ as a function of h_x, and the critical value is $h_{x,c}/J = 0.0712$. Thus, it is estimated as $h_{x,c}/J = 0.071 \pm 0.0003$, which causes the error bars in Fig. 2(a).

Next we consider the XXZ model with XY anisotropy,

$$\mathcal{H} = \mathcal{H}_{\rm XXZ} + D_{xy} \sum_j (S_j^x S_{j+1}^x - S_j^y S_{j+1}^y). \tag{7}$$

This Hamiltonian is nothing but the XYZ model, which is exactly solvable [28]. Staggered magnetization $m_{\rm N}^x$ and $m_{\rm N}^z$ calculated by iTEBD is shown in Fig. 1(b). In contrast to Fig. 1(a), the orders $m_{\rm N}^x$ and $m_{\rm N}^z$ are exclusively competing, i.e., if one of the two orders is nonzero, the other is zero. The critical value of D_{xy} is $D_{xy,c} = (\Delta - 1)J$. Since $J - D_{xy,c} < J + D_{xy,c} = \Delta J$, the Hamiltonian is the easy-plane XXZ model at the critical point and the ground state is Tomonaga-Luttinger liquid (a conformal field theory with central charge $c = 1$). Hence the transition is the BKT type, which is consistent with the renormalization analysis [10].

IV. DYNAMICAL SUSCEPTIBILITY

Let us now compute how the critical behavior of the models of Sec. III can be measured experimentally. In addition to the static staggered magnetization, we show that the dynamical susceptibility captures well the properties of the quantum phase transition. This quantity is directly accessible in INS and ESR experiments.

The spin-spin retarded correlation function is defined as

$$\chi^{\alpha\beta}(\boldsymbol{r}, t) = -i\vartheta_{\rm step}(t)\langle[S_{\boldsymbol{r}}^{\alpha}(t), S_0^{\beta}(0)]\rangle, \tag{8}$$

where $\vartheta_{\rm step}(t)$ is the Heaviside function. For 1D lattice systems, $\boldsymbol{r}$ is replaced with the site index j. The dynamical susceptibility is obtained from the Fourier transform of the retarded correlation function (8),

$$\chi^{\alpha\beta}(\boldsymbol{q}, \omega) = \int_{-\infty}^{\infty} dt \sum_{\boldsymbol{r}} e^{i(\omega t - \boldsymbol{q}\cdot\boldsymbol{r})} \chi^{\alpha\beta}(\boldsymbol{r}, t) \tag{9}$$

This quantity is related to the differential scattering cross section of INS by

$$\frac{d^2\sigma}{d\Omega dE} \propto \frac{|\boldsymbol{q}_{\rm out}|}{|\boldsymbol{q}_{\rm in}|} |F(\boldsymbol{Q})|^2 \sum_{\alpha,\beta=x,y,z} \left(\delta_{\alpha\beta} - \frac{Q_\alpha Q_\beta}{|\boldsymbol{Q}|^2}\right) \times {\rm Im}\chi^{\alpha\beta}(\boldsymbol{Q}, \omega), \tag{10}$$

where $F(\boldsymbol{Q})$ is the magnetic form factor and $\boldsymbol{q}_{\rm in}$, $\boldsymbol{q}_{\rm out}$ is the direction of incoming and outgoing fluxes, respectively. $\boldsymbol{Q}$ is a scattering vector defined as $\boldsymbol{Q} = \boldsymbol{q}_{\rm in} - \boldsymbol{q}_{\rm out}$. If the system is $U(1)$ symmetric (i.e., $\sum_j S_j^z$ is conserved), Eq. (10) is rewritten as [29]

$$\frac{d^2\sigma}{d\Omega dE} \propto \frac{|\boldsymbol{q}_{\rm out}|}{|\boldsymbol{q}_{\rm in}|} |F(\boldsymbol{Q})|^2 \Big\{ \Big(1 - \frac{Q_z^2}{|\boldsymbol{Q}|^2}\Big) {\rm Im}\chi^{zz}(\boldsymbol{Q}, \omega) + \Big(1 + \frac{Q_z^2}{|\boldsymbol{Q}|^2}\Big) {\rm Im}\chi^{xx}(\boldsymbol{Q}, \omega) \Big\}, \tag{11}$$

since $\chi^{xx} = \chi^{yy}$. In ESR experiments, since electromagnetic waves in the GHz frequency region are used, the wavelength is much larger than the lattice constant and only the response at $|\boldsymbol{q}| = 0$ is relevant. When such electromagnetic waves are applied to the system, the energy absorption rate is given by

$$I(\omega) \propto \omega {\rm Im}\chi^{\alpha\alpha}(\boldsymbol{q} = 0, \omega), \tag{12}$$

where α is the direction of oscillating magnetic field. $I(\omega)$ corresponds with spectrum of ESR.

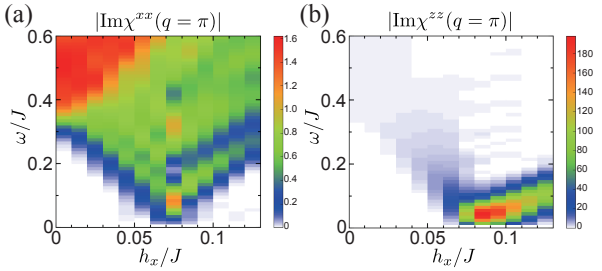

FIG. 4. Dynamical susceptibility (a) $\chi^{xx}(q=\pi)$ and (b) $\chi^{zz}(q=\pi)$ for the XXZ model ($\Delta=1.9$) with staggered x field. The dominant low energy excitation in the low (high) h_x phase corresponds to χ^{xx} (χ^{zz}). We see that χ^{zz} diverges at the transition point $h_x/J\simeq 0.071$ while χ^{xx} does not.

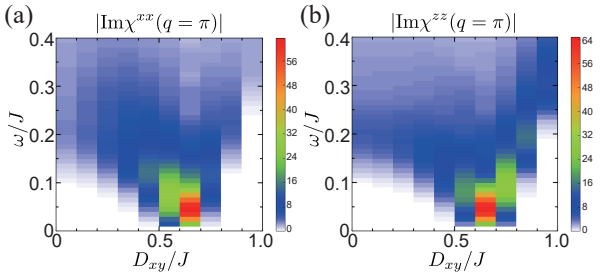

FIG. 5. Dynamical susceptibility (a) $\chi^{xx}(q=\pi)$ and (b) $\chi^{zz}(q=\pi)$ for the XXZ model ($\Delta=1.6$) with XY anisotropy. Both χ^{xx} and χ^{zz} diverge at the transition point $D_{xy}/J=0.6$.

We compute the dynamical susceptibility numerically. We first obtain the ground state of the system by infinite density matrix renormalization group (iDMRG) [30], then perform the time evolution by iTEBD [31] with the infinite boundary condition [32]. In this way, we can calculate space-time correlation function $\langle S^{\alpha}_{\boldsymbol{r}}(t)S^{\beta}_{0}(0)\rangle$, and dynamical susceptibility through Fourier transform. The details of numerical calculation are given in Appendix A.

In Fig. 4, we show the dynamical susceptibility at $q=\pi$ in the XXZ model with staggered x field (5). In the low (high) h_x phase, the dominant low energy elementary excitation corresponds to χ^{xx} (χ^{zz}). The order is in the z direction at $h_x=0$, and m^z_{N} decreases while m^x_{N} increases as h_x becomes larger. Above the critical h_x, the order is in the x direction. Hence the behavior of χ^{xx} and χ^{zz} indicates that the low energy excitation is generated by a spin flip. We can also see that χ^{zz} diverges at the transition point while χ^{xx} does not in Fig. 4. That is because m^z_{N} becomes zero at the transition point while m^x_{N} changes smoothly. [see Fig. 1(a)].

Let us now compare with the dynamical susceptibility at $q=\pi$ for the XXZ model with XY anisotropy (7) in Fig. 5. Similarly to the staggered x field case, in the low (high) D_{xy} phase, the dominant elementary excitation corresponds to χ^{xx} (χ^{zz}). There are however an important difference on the susceptibilities, which stems from

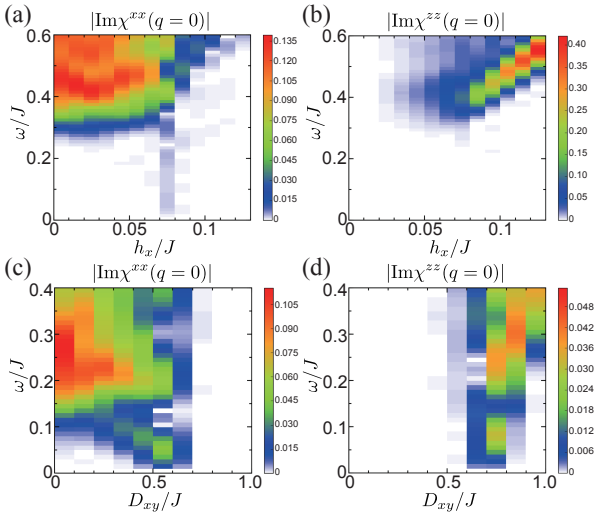

FIG. 6. Dynamical susceptibility (a) $\chi^{xx}(q=0)$ and (b) $\chi^{zz}(q=0)$ for the XXZ model ($\Delta=1.9$) with staggered x field and (c) $\chi^{xx}(q=0)$ and (d) $\chi^{zz}(q=0)$ for the XXZ model ($\Delta=1.6$) with XY anisotropy.

the different nature of the transition. It is directly visible that both χ^{xx} and χ^{zz} diverge at the transition point in Fig. 5. This is the consequence of the exclusive competition between m^x_{N} and m^z_{N}, both of which become zero at the transition point [see Fig. 1(b)].

We also discuss the dynamical susceptibility at $q=0$ which is relevant with ESR experiments. Figure 6 shows $\chi^{xx}(q=0)$ and $\chi^{zz}(q=0)$ for the XXZ model ($\Delta=1.9$) with staggered x field and with XY anisotropy. We first note that the intensity of the dynamical susceptibility is extremely small at $q=0$ compared with $q=\pi$ since antiferromagnetic correlation is dominant in the present system. As seen in Figs. 6(a) and (b), gap does not close at $q=0$ for the XXZ model with staggered x field. Small intensity of the low energy region ($\omega/J\lesssim 0.3$) near the critical field $h_x\simeq 0.07$ is numerical artifact. On the contrary, Figs. 6(c) and (d) show that gap closes at $q=0$ for the XXZ model with XY anisotropy. This is natural since the critical point corresponds to an easy plain XXZ model and the gapless des Cloizeaux-Pearson mode exists at $q=0$.

As for the XXZ model with staggered x field, the band at $q=\pi$ is folded to the band at $q=0$ due to the perturbation that breaks one-site translational symmetry. Thus, ESR measurements captures the mixing of $q=0$ and $q=\pi$ components of dynamical susceptibility. This effect is seen in Cu benzoate [33], $KCuGaF_6$ [34], and $BaCo_2V_2O_8$ [35]. The similar mixing is also measured in $(C_7H_{10}N)_2CuBr_4$ [36].

The above calculations clarifies that the spin-spin susceptibility shows very clear signatures of the nature of these two different topological transitions. Although these measurements do not directly give access to the nonlocal (topological) order, they nevertheless provide

clear signatures of the change of the nature of the excitations.

V. APPLICATION TO REAL MATERIALS

In the above, we discussed the models that can be mapped to DDSG models and their quantum phase transitions. In order to apply the above theoretical analysis to realistic materials, one has to consider several important elements depending on whether the system is condensed matter or cold atomic gas.

A. Condensed matter systems

For the condensed matter realizations, two elements are to be taken into account. First, in the present experiments, one can expect to measure only the local observable (magnetization, spin-spin susceptibility, etc.). Nonlocal order parameters (e.g., $\cos(\theta(x)/2)$ in Sec. II A) are difficult to measure experimentally in condensed matter systems. Second, in quasi-1D materials, spin chains are coupled and form three dimensional system while the analysis done in the previous parts is strictly 1D.

Recently, the DDSG model discussed above was found to be realized in the compound $BaCo_2V_2O_8$ [19]. In this material, Co^{2+} ions effectively form the $S = 1/2$ quasi-1D antiferromagnet with Ising anisotropy. When an external magnetic field perpendicular to the anisotropy axis is applied in this system, an effective staggered transverse field arises since nondiagonal components of g tensor are nonzero due to the slight deviation of the magnetic principal axes from the crystallographic axes [37]. The model Hamiltonian of this compound is essentially equivalent to the XXZ model with staggered x field (5), and the quantum phase transition discussed in Sec. II A happens. Note that an effective staggered field $-h_{\rm eff}\sum_j(-1)^j S^z_j$ along the z axis arises from the interchain interaction, determined self-consistently, with the Néel order along the z axis in the mean field theory has also to be taken into account [19]. Due to this staggered z field, the critical field is shifted to a higher value than the case without the interchain interaction and the gap opens at the transition point with $h_{\rm eff} = 0$. Thus, the gap is not closed at the quantum phase transition caused by the transverse field in $BaCo_2V_2O_8$. As discussed in Sec. IV, the dynamical susceptibility is measured by INS experiments. For a direct comparison with the neutrons, one has to use the actual position of the spin sites (the Co^{2+} ions) in the Fourier transform of retarded correlation function since the neutrons are directly sensitive to the actual position of the spins.

It would be interesting if other examples of the topological transitions discussed in the previous sections also could be realized. The potential of the field ϕ is provided by dimerization, Ising anisotropy, and staggered Dzyaloshinskii-Moriya (DM) interaction $\sum_j(-1)^j \boldsymbol{D}\cdot(\boldsymbol{S}_j\times\boldsymbol{S}_{j+1})$ with $D \parallel z$ axis. The strategy for material search is to find systems that have these perturbations as well as nondiagonal staggered g tensor. The application of effective staggered field introduces effective staggered field, which gives the potential of the field θ. Then the transition is provoked by increasing the external field. In addition to spin chains, searching for materials which realize the DDSG model in spin ladders with magnetic anisotropy or DM interaction is an interesting future direction.

B. Cold atomic systems

Another important route to realize the topological transitions described in the previous sections is provided by cold atomic systems [38, 39]. Although initial simulations of quantum magnetism were done in bosonic systems by using the mapping between spin-1/2 and hard core bosons [40, 41] and thus the realization is limited to XX models due to the absence of long range interactions, recent advance allows to probe the quantum magnetism in fermionic systems as well. Short-range quantum magnetism has been observed for ultracold fermions in an optical lattice [42], and measurements of various physical quantities such as dynamical structure factor [43] and magnetic order and correlations [44–46]. In addition to systems with fermions, quantum simulation of spin systems are also realized by using Rydberg atoms [47, 48].

There are several advantages for the cold atomic realization. The first is the controllability of parameters. While the parameters are fixed for each material in condensed matter systems, particle-particle interaction can be varied by using Feshbach resonance in cold atomic systems. Controlling the population of up-spins and down-spins allows the equivalent of a magnetic field along z. The second advantage is that cold atomic systems provide the probes complementary to the condensed matter ones, in particular to measure nonlocal order parameters. For example, a string order parameter in the Haldane phase can be observed by repeating snapshot measurements [49] in cold atomic systems. This technique can be also potentially applicable for measuring nonlocal order parameters such as $\cos(\theta(x)/2)$ discussed in Sec. II A. Measurements are so far limited to equal time correlations but schemes have been proposed to overcome such limitations [50].

One of the challenges in this field is cooling the system enough to simulate the low temperature phenomena of the corresponding condensed matter systems. However, since the experimental technique of cooling has been improving [51], we can expect that some of the phases described here could be observed in the near future.

VI. CONCLUSION

We studied quantum phase transitions between competing orders in the models which is mapped to the DDSG field theory. We specifically considered two types of systems: the XXZ chain with staggered x field and with XY anisotropy. The universality class of the transition is of the Ising type in the former case while it is of the BKT type in the latter case. We showed numerically that the difference of the transition properties appears in the dynamical susceptibilities, which can be directly compared with the spectra measured by INS experiments. We discussed the possibility of observation of the phases and the phase transitions studied in the present paper in condensed matter systems and cold atomic ones. For condensed matter realizations, one of the quantum phase transition between competing orders has been seen in a real material $BaCo_2V_2O_8$, which is a quasi-1D Heisenberg antiferromagnet with Ising anisotropy [19]. Other quantum spin systems either chains or ladders with anisotropic perturbations could serve as a basis for studying the other universality classes discussed here. In that respect the dynamical susceptibilities, directly measured by INS or ESR experiments, computed in the present paper, provide a clear distinction between the various transitions and can thus be used as an experimental signature.

Another broad class of systems in which the phenomena can be investigated is provided by cold atomic systems of fermions or Rydberg atoms. Such systems have the advantage of a good control of the various parameters in the Hamiltonian as well as the possibility of measure the nonlocal (topological) order parameters which are a direct signature of the various phases. Relatively high temperature as well as the size limitation is the current drawbacks, but the situation is rapidly evolving. These systems also offer the fascinating possibility to study time-dependent Hamiltonians, allowing to investigate the effect of time dependent perturbations in the future, either quenches or periodic perturbations (Floquet systems) on such topological phase transitions.

ACKNOWLEDGMENTS

The authors gratefully thank the many fruitful discussions with Q. Faure, B. Grenier, S. Petit, V. Simonet and Ch. Rüegg on quantum spin chains. S. T. is supported by the Swiss National Science Foundation under Division II and ImPact project (No. 2015-PM12-05-01) from the Japan Science and Technology Agency. S. C. F. is supported by JSPS KAKENHI (No. JP16J04731).

Appendix A: Details of numerical simulations

In this appendix, we describe the detail of numerical simulations. Time evolution is calculated by iTEBD [31] after the ground state is obtained by iDMRG [30]. The iTEBD uses the MPS representation of quantum states, and the time evolving operator is applied through the second order Trotter decomposition. Time is discretized with the unit $dt/J^{-1} = 0.05$ in this study. The initial state (ground state) is represented as infinite MPS, which assumes translational invariance of the system, but in order to calculate the space-time correlation function, we have to break the translational invariance by applying an operator at $t = 0, j = 0$. Thus, we prepare a finite spatial interval and the matrices at both edges of the interval is determined in the way that they represent a semi-infinite extension of the system, which is called the infinite boundary condition [32]. The advantage of this method is that there is no finite-size effect. The space-time correlation function Eq. (8) is calculated for a finite temporal interval $0 \le t \le T$, and dynamical susceptibility is obtained as the numerical Fourier transform of the space-time correlation function. Gaussian filter is utilized in the Fourier transformation,

$$\chi(q,\omega) = \int_{-T}^{T} dt \sum_r e^{i(\omega t - qr)} \chi(r,t) G(t),$$

where $G(t) = e^{-(2t/T)^2}$.

In the iTEBD and iDMRG calculations, quantum states are optimally approximated by MPS with finite bond dimension (also called truncation dimension) M. As the bond dimension M is larger, the calculation is more precise. In Fig. 7(a), we show $\chi^{xx}(q = \pi, \omega)$ calculated with Eq. (5) for different bond dimensions $M = 40, 60, 80$ while $T/J^{-1} = 80$ is fixed. We can see that the dependence of the result on M is small. In the real-time calculation, an error also arises from a finite time effect. Figure 7(b) shows $\chi^{xx}(q = \pi, \omega)$ calculated with Eq. (5) for final time $T/J^{-1} = 40, 60, 80$ while $M = 60$ is fixed. The dependence of the result on T is also small.

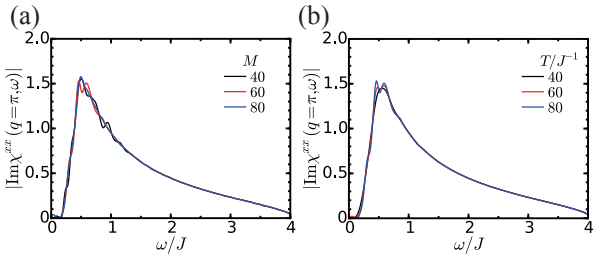

FIG. 7. The dependence of iTEBD calculations (a) on the truncation dimension M with fixed $T/J^{-1} = 80$ and (b) on the temporal interval T with fixed $M = 60$. The results of $\mathrm{Im}\chi^{xx}(q = \pi, \omega)$ for the model (5) are shown with $\Delta = 1.9$ and $h_x/J = 0.02$.

[1] V. L. Berezinskii, Sov. Phys. JETP **32**, 493 (1971).
[2] V. L. Berezinskii, Sov. Phys. JETP **34**, 610 (1972).
[3] J. M. Kosterlitz and D. J. Thouless, J. Phys. C: Solid State Phys. **6**, 1181 (1973).
[4] T. Giamarchi, *Quantum physics in one dimension* (Oxford university press, Oxford, 2004).
[5] M. Oshikawa and I. Affleck, Phys. Rev. Lett. **79**, 2883 (1997).
[6] I. Affleck and M. Oshikawa, Phys. Rev. B **60**, 1038 (1999).
[7] D. C. Dender, P. R. Hammar, D. H. Reich, C. Broholm, and G. Aeppli, Phys. Rev. Lett. **79**, 1750 (1997).
[8] F. D. M. Haldane, Phys. Lett. A **93**, 464 (1983).
[9] F. D. M. Haldane, Phys. Rev. Lett. **50**, 1153 (1983).
[10] T. Giamarchi and H. J. Schulz, J. Phys. France **49**, 819 (1988).
[11] P. Lecheminant, A. O. Gogolin, and A. A. Nersesyan, Nucl. Phys. B **639**, 502 (2002).
[12] G. Delfino, "Field theory of scaling lattice models: The potts antiferromagnet," in *Statistical Field Theories*, edited by A. Cappelli and G. Mussardo (Springer Netherlands, Dordrecht, 2002) pp. 3–12.
[13] S. Sarkar, Sci. Rep. **6**, 30569 (2016).
[14] J. V. José, L. P. Kadanoff, S. Kirkpatrick, and D. R. Nelson, Phys. Rev. B **16**, 1217 (1977).
[15] H. A. Fertig, Phys. Rev. Lett. **89**, 035703 (2002).
[16] E. Orignac, R. Citro, M. Di Dio, and S. De Palo, Phys. Rev. B **96**, 014518 (2017).
[17] R. Citro, S. De Palo, M. Di Dio, and E. Orignac, Phys. Rev. B **97**, 174523 (2018).
[18] N. J. Robinson, A. Altland, R. Egger, N. M. Gergs, W. Li, D. Schuricht, A. M. Tsvelik, A. Weichselbaum, and R. M. Konik, arXiv:1806.01925 (2018).
[19] Q. Faure, S. Takayoshi, S. Petit, V. Simonet, S. Raymond, L.-P. Regnault, M. Boehm, J. S. White, M. Månsson, C. Rüegg, P. Lejay, B. Canals, T. Lorenz, S. C. Furuya, T. Giamarchi, and B. Grenier, Nat. Phys. **14**, 716 (2018).
[20] S. R. White, Phys. Rev. Lett. **69**, 2863 (1992).
[21] T. Hikihara and A. Furusaki, Phys. Rev. B **69**, 064427 (2004).
[22] S. Takayoshi and M. Sato, Phys. Rev. B **82**, 214420 (2010).
[23] P. Bouillot, C. Kollath, A. M. Läuchli, M. Zvonarev, B. Thielemann, C. Rüegg, E. Orignac, R. Citro, M. Klanjšek, C. Berthier, M. Horvatić, and T. Giamarchi, Phys. Rev. B **83**, 054407 (2011).
[24] T. Hikihara, A. Furusaki, and S. Lukyanov, Phys. Rev. B **96**, 134429 (2017).
[25] E. Berg, E. G. Dalla Torre, T. Giamarchi, and E. Altman, Phys. Rev. B **77**, 245119 (2008).
[26] P. Calabrese and J. Cardy, J. Stat. Mech. **2004**, P06002 (2004).
[27] A. M. Tsvelik and A. B. Kuklov, New J. Phys. **14**, 115033 (2012).
[28] R. J. Baxter, *Exactly solved models in statistical mechanics* (Elsevier, Amsterdam, 2016).
[29] S. W. Lovesey, *Theory of neutron scattering from condensed matter* (Oxford university press, Oxford, 1986).
[30] I. P. McCulloch, arXiv:0804.2509 (2008).
[31] G. Vidal, Phys. Rev. Lett. **98**, 070201 (2007).
[32] H. N. Phien, G. Vidal, and I. P. McCulloch, Phys. Rev. B **86**, 245107 (2012).
[33] M. Oshikawa and I. Affleck, Phys. Rev. B **65**, 134410 (2002).
[34] S. C. Furuya and M. Oshikawa, Phys. Rev. Lett. **109**, 247603 (2012).
[35] S. Kimura, H. Yashiro, K. Okunishi, M. Hagiwara, Z. He, K. Kindo, T. Taniyama, and M. Itoh, Phys. Rev. Lett. **99**, 087602 (2007).
[36] M. Ozerov, M. Maksymenko, J. Wosnitza, A. Honecker, C. P. Landee, M. M. Turnbull, S. C. Furuya, T. Giamarchi, and S. A. Zvyagin, Phys. Rev. B **92**, 241113 (2015).
[37] S. Kimura, K. Okunishi, M. Hagiwara, K. Kindo, Z. He, T. Taniyama, M. Itoh, K. Koyama, and K. Watanabe, J. Phys. Soc. Jpn. **82**, 033706 (2013).
[38] I. Bloch, J. Dalibard, and W. Zwerger, Rev. Mod. Phys. **80**, 885 (2008).
[39] H. Ritsch, P. Domokos, F. Brennecke, and T. Esslinger, Rev. Mod. Phys. **85**, 553 (2013).
[40] J. Struck, C. Ölschläger, R. Le Targat, P. Soltan-Panahi, A. Eckardt, M. Lewenstein, P. Windpassinger, and K. Sengstock, Science **333**, 996 (2011).
[41] E. Y. Vedmedenko, M. Schult, J. Kronjager, R. Wiesendanger, K. Bongs, and K. Sengstock, New J. Phys. **15**, 063033 (2013).
[42] D. Greif, T. Uehlinger, G. Jotzu, L. Tarruell, and T. Esslinger, Science **340**, 1307 (2013).
[43] R. Landig, F. Brennecke, R. Mottl, T. Donner, and T. Esslinger, Nat. Comm. **6**, 7046 (2015).
[44] M. F. Parsons, A. Mazurenko, C. S. Chiu, G. Ji, D. Greif, and M. Greiner, Science **353**, 1253 (2016).
[45] M. Boll, T. A. Hilker, G. Salomon, A. Omran, J. Nespolo, L. Pollet, I. Bloch, and C. Gross, Science **353**, 1257 (2016).
[46] L. W. Cheuk, M. A. Nichols, K. R. Lawrence, M. Okan, H. Zhang, E. Khatami, N. Trivedi, T. Paiva, M. Rigol, and M. W. Zwierlein, Science **353**, 1260 (2016).
[47] A. Browaeys, D. Barredo, and T. Lahaye, J. Phys. B: At. Mol. Opt. Phys. **49**, 152001 (2016).
[48] V. Lienhard, S. de Léséleuc, D. Barredo, T. Lahaye, A. Browaeys, M. Schuler, L.-P. Henry, and A. M. Läuchli, Phys. Rev. X **8**, 021070 (2018).
[49] M. Endres, M. Cheneau, T. Fukuhara, C. Weitenberg, P. Schauß, C. Gross, L. Mazza, M. C. Bañuls, L. Pollet, I. Bloch, and S. Kuhr, Science **334**, 200 (2011).
[50] M. Knap, A. Kantian, T. Giamarchi, I. Bloch, M. D. Lukin, and E. Demler, Phys. Rev. Lett. **111**, 147205 (2013).
[51] A. Mazurenko, C. S. Chiu, G. Ji, M. F. Parsons, M. Kanász-Nagy, R. Schmidt, F. Grusdt, E. Demler, D. Greif, and M. Greiner, Nature **545**, 462 (2017).